Int. J. Solids Structures, 1971, Vol. 7, pp. 1031 to 1055. Pergamon Press. Printed in Great Britain

MODAL REPRESENTATIONS FOR THE HIGH-FREQUENCY RESPONSE OF ELASTIC PLATES

P. W. RANDLES†

University of Colorado

and

J. MIKLOWITZ‡

California Institute of Technology

Abstract—High-frequency representations for the response of an infinite plate to an impulsive line load are extracted from a new form of the usual modal solution. A change of variables is used to facilitate an investigation of the branches of the Rayleigh–Lamb frequency equation. Branch points of the branches are found about which analytic continuations are made, which lead to the new form of the modal solution and which uncouple the dilatational and equivoluminal motion. Singular wave fronts are investigated and certain terms in the final solution, approximated with high-frequency series representations for the branches, are evaluated and compared with known half space solutions. The method is applicable to certain anisotropic materials; however, a homogeneous, isotropic plate is treated.

1. INTRODUCTION

THIS work is concerned with representations for the high-frequency response of a suddenly loaded infinite plate governed by the equations of motion from linear elasticity theory. The problem has been given attention in the literature only recently. The method of attack has almost exclusively exploited Cagniard's method, geometric ray theory and wave front expansions, as the most recent of these, that by Rosenfeld and Miklowitz [1], exhibits. On the other hand, in the present work high-frequency representations are extracted from the modal form of the solution, which is based on the underlying frequency spectrum. The method is conveniently applicable to a broader class of problems than is Cagniard's method, including wave propagation in anisotropic plates and possibly in layered media and circular rods.

The method and representations are brought forth by treating the problem of an infinite plate, subjected to an impulsive line load applied normal to one of the faces, which are otherwise free. The plate material is isotropic and homogeneous.

The modal form of the exact solution is recounted in Section 2 and it consists of an infinite sum of integrals, each of which represents a mode of propagation. The modes are directly related to the branches, or roots, of the Rayleigh–Lamb frequency equation, which gives a functional relationship between the frequency and wave number of straight-crested waves propagating in the plate. The frequency spectrum, a plot of frequency

† Assistant Professor of Mechanical Engineering.
‡ Professor of Applied Mechanics.

versus wave number, is now quite well understood, chiefly through the recent efforts of Mindlin *et al.* (see [2]). However, this knowledge is not sufficient for the present problem in which an understanding of the relationship between the high-frequency portion of the frequency spectrum and the high-frequency response of the plate is required.

The variables in the modal solution are changed in Section 3 as a necessary step to solve this problem. In the new variables, an extension of Mindlin's investigation [2] of the branches of the frequency equation is given in Section 4. The most important new result, which relates to the high-frequency response, is the existence of analytic continuations of the branches which are closely associated with the dilatational waves in the plate, and which are crucial to this work. These are called the dilatational branches and they are found with both the frequency and wave number pure imaginary. Branch points and analytic continuations of the branches are investigated for use in high-frequency representations. Also, series representations, valid for high frequency, for the dilatational branches and for the familiar branches of the frequency equation, called equivoluminal branches here, are developed.

In Section 5 an equivalent modal solution is derived, which involves integrals over the equivoluminal and dilatational branches. This modal solution uncouples the equivoluminal and dilatational motion which results from reflections at the free faces of the plate and is the major complicating factor in these problems.

The equivalent modal solution is approximated, in Section 6, by using the series representations for the branches. This being done, the summations over the mode numbers are carried out and the expected geometry of the singular wave fronts is recognized in Section 7. Example terms are evaluated in Section 8 for comparison with known half space solutions.

2. THE MODAL SOLUTION FOR THE PLATE LINE LOAD PROBLEM

The plane strain equations of motion of linear elasticity for an isotropic homogeneous material are

$$\begin{aligned} \frac{\partial^2\phi}{\partial x_1^2}+\frac{\partial^2\phi}{\partial x_3^2} &= \frac{1}{c_1^2}\frac{\partial^2\phi}{\partial t^2}, \\ \frac{\partial^2\psi}{\partial x_1^2}+\frac{\partial^2\psi}{\partial x_3^2} &= \frac{1}{c_2^2}\frac{\partial^2\psi}{\partial t^2}, \end{aligned} \tag{1}$$

where $\phi(x_1, x_3, t)$ is the scalar dilatational potential and $\psi(x_1, x_3, t)$ is the x_2 component of the vector equivoluminal potential. x_1, x_2 and x_3 are rectangular Cartesian coordinates and the x_1 and x_3 components of displacement are given by

$$\begin{aligned} u &= \frac{\partial\phi}{\partial x_1}-\frac{\partial\psi}{\partial x_3}, \\ w &= \frac{\partial\phi}{\partial x_3}+\frac{\partial\psi}{\partial x_1}, \end{aligned} \tag{2}$$

respectively. The dilatational and equivoluminal body wave velocities are

$$c_1 = [(\lambda+2\mu)/\rho]^{\frac{1}{2}}, \qquad c_2 = (\mu/\rho)^{\frac{1}{2}} \tag{3}$$

where λ and μ are the Lamé constants and ρ is the density of the material. The ratio

$$a = c_1/c_2 = [2(1-\nu)/(1-2\nu)]^{\frac{1}{2}} \tag{4}$$

is used as an elastic constant along with Poisson's ratio ν, which is restricted to the range $0 < \nu < \frac{1}{2}$ in this work.

Figure 1 shows the geometry of the plate line load problem and the equations of motion are to be solved in the interior, $-\infty < x_1 < \infty$ and $-H < x_3 < H$, of the plate. The solution is subject to the boundary conditions

$$\begin{aligned} \sigma_{33}(x_1, H, t) &= -I\delta(x_1)\delta_+(t), \\ \sigma_{33}(x_1, -H, t) &= 0, \\ \sigma_{13}(x_1, \pm H, t) &= 0 \end{aligned} \tag{5}$$

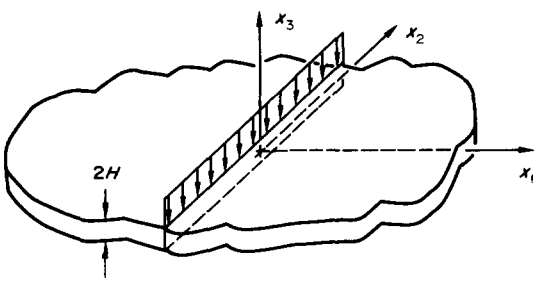

FIG. 1. Plate line load problem.

where

$$\sigma_{33} = (\lambda+2\mu)\frac{\partial w}{\partial x_3} + \lambda\frac{\partial u}{\partial x_1} \quad \text{and} \quad \sigma_{13} = \mu\left(\frac{\partial u}{\partial x_3} + \frac{\partial w}{\partial x_1}\right)$$

are the pertinent stresses for this problem. $\delta(x_1)$ is the Dirac delta function and $\delta_+(t)$ is the one-sided delta function. The delta functions are localized at $x_1 = 0$ and $t = 0$ and defined so that

$$\int_{x_1=-\infty}^{\infty}\int_{t=0}^{\infty} \sigma_{33}(x_1, H, t)\,\mathrm{d}t\,\mathrm{d}x_1 = -I,$$

with the constant I being the impulse per unit length along the line of loading. Also, the plate is quiescent for $t \leq 0$ and the radiation condition requires that all dependent variables vanish as $|x_1| \to \infty$.

This problem is easily solved, formally at least, by applying a Laplace transform on t and a Fourier transform on x_1 to the differential equations (1) and to the boundary and initial conditions and then inverting the solution. This leaves a double integral representation which can be replaced with an infinite sum of single integrals (the modal solution) by using residue calculus.

The modal solution for a symmetrical line load with respect to the midplane of the plate was given by Lloyd and Miklowitz [3] and the asymmetrical line load solution is

obtained similarly. Since the loading (5) can be decomposed into a symmetrical and an asymmetrical loading, the derivation of the modal solution is not repeated here.

The facts that the equations of motion (1) are hyperbolic and that (5) is an impulsive line load insures that $u = w = 0$ for $t < [x_1^2+(H-x_3)^2]^{\frac{1}{2}}/c_1$. For $t \geq [x_1^2+(H-x_3)^2]^{\frac{1}{2}}/c_1$ the displacement components are given by the modal solution

$$u(x_1, x_3, t) = \frac{I}{\pi\mu}\sum_{n=0}^{\infty}\int_0^{\infty} \varkappa \sin(\varkappa x_1)\sin(\omega t)\left.\frac{\tilde{u}_{(+)}}{\dfrac{\partial F_{(+)}}{\partial\omega}}\right|_{\substack{F_{(+)}=0\\ \omega=\omega_n(\varkappa)}} d\varkappa$$

$$+\frac{I}{\pi\mu}\sum_{n=0}^{\infty}\int_0^{\infty} \varkappa \sin(\varkappa x_1)\sin(\omega t)\left.\frac{\tilde{u}_{(-)}}{\dfrac{\partial F_{(-)}}{\partial\omega}}\right|_{\substack{F_{(-)}=0\\ \omega=\omega_n(\varkappa)}} d\varkappa, \tag{6}$$

$$w(x_1, x_3, t) = \frac{I}{\pi\mu}\sum_{n=0}^{\infty}\int_0^{\infty} \alpha \cos(\varkappa x_1)\sin(\omega t)\left.\frac{\tilde{w}_{(+)}}{\dfrac{\partial F_{(+)}}{\partial\omega}}\right|_{\substack{F_{(+)}=0\\ \omega=\omega_n(\varkappa)}} d\varkappa$$

$$-\frac{I}{\pi\mu}\sum_{n=0}^{\infty}\int_0^{\infty} \alpha \cos(\varkappa x_1)\sin(\omega t)\left.\frac{\tilde{w}_{(-)}}{\dfrac{\partial F_{(-)}}{\partial\omega}}\right|_{\substack{F_{(-)}=0\\ \omega=\omega_n(\varkappa)}} d\varkappa$$

where

$$\alpha = (\omega^2/c_1^2-\varkappa^2)^{\frac{1}{2}}, \qquad \beta = (\omega^2/c_2^2-\varkappa^2)^{\frac{1}{2}}, \tag{7}$$

$$F_{(+)} = \frac{2}{(\beta+\alpha)^2}[(\omega^2/c_2^2-2\varkappa^2)^2\cos(\alpha H)\sin(\beta H)+4\varkappa^2\alpha\beta\sin(\alpha H)\cos(\beta H)],$$

$$F_{(-)} = \frac{2}{(\beta+\alpha)^2}[(\omega^2/c_2^2-2\varkappa^2)^2\sin(\alpha H)\cos(\beta H)+4\varkappa^2\alpha\beta\cos(\alpha H)\sin(\beta H)], \tag{8}$$

$$\tilde{u}_{(+)} = \frac{2}{(\beta+\alpha)^2}[(\omega^2/c_2^2-2\varkappa^2)\cos(\alpha x_3)\sin(\beta H)-2\alpha\beta\sin(\alpha H)\cos(\beta x_3)],$$

$$\tilde{u}_{(-)} = \frac{2}{(\beta+\alpha)^2}[(\omega^2/c_2^2-2\varkappa^2)\sin(\alpha x_3)\cos(\beta H)-2\alpha\beta\cos(\alpha H)\sin(\beta x_3)], \tag{9}$$

$$\tilde{w}_{(+)} = \frac{2}{(\beta+\alpha)^2}[(\omega^2/c_2^2-2\varkappa^2)\sin(\alpha x_3)\sin(\beta H)+2\varkappa^2\sin(\alpha H)\sin(\beta x_3)],$$

$$\tilde{w}_{(-)} = \frac{2}{(\beta+\alpha)^2}[(\omega^2/c_2^2-2\varkappa^2)\cos(\alpha x_3)\cos(\beta H)+2\varkappa^2\cos(\alpha H)\cos(\beta x_3)].$$

The (+) and (−) subscripts identify terms with the response to the symmetrical and asymmetrical loadings, respectively, in the decomposition of (5). The familiar Rayleigh–

Lamb frequency equation is given by $F_{(\pm)} = 0$ and it admits an infinite set of real branches for $0 < \varkappa < \infty$. Both the symmetrical and asymmetrical positive branches are denoted by $\omega_n(\varkappa)$ and they are ordered so that $\omega_n(\varkappa) < \omega_{n+1}(\varkappa)$ for $n = 0, 1, 2 \ldots$ and $0 < \varkappa < \infty$. These branches have been treated in detail by Mindlin [2]. The functions (9) are written so that the first term in each results from the dilatational potential ϕ and the second term results from the equivoluminal potential ψ by (2).

The integration over $\varkappa$ and the summation over n have been interchanged in deriving (6) even though the loading (5) is expected to produce singular wave fronts. Either the integrals or the sums must diverge to produce these singularities. Thus, if theorems requiring uniform convergence are to be used to justify this interchange, either the loading must be made smoother or the generalized functions in (5) must be replaced by defining sequences with the limits to the generalized functions taken after these integrations and summations are carried out. The latter is the most direct way to show that (6) is the response of the plate to the loading (5).

3. THE MODAL SOLUTION IN NEW VARIABLES

Much of the high-frequency response of the plate, which must be contained in the representation (6), is apparently inaccessible through direct integration and summation even when approximations such as asymptotic expansions are employed. In order to make the modal solution and the underlying frequency spectrum [made up of the branches $\omega_n(\varkappa)$ for $0 \leq \varkappa \leq \infty$] more easily handled with tools such as analytic function theory, the variables

$$\chi = (\beta - \alpha)/(\beta + \alpha), \qquad \eta = H(\beta + \alpha) \tag{10}$$

are introduced with χ replacing the integration variable $\varkappa$ in (6). This choice of variables is similar to Holden's choice [4] of α and β to replace $\varkappa$ and ω for study of the branches of the frequency equation. However, χ and η allow a more direct approach to the high-frequency response of the plate than either α and β or $\varkappa$ and ω. χ and η are uniquely defined by taking $\alpha = |\alpha|$ when α is real and $\beta = |\beta|$ when β is real and $\alpha = -i|\alpha|$ and $\beta = -i|\beta|$ when they are pure imaginary.

The inverses of (10) are

$$\begin{aligned} \alpha &= \eta(1-\chi)/2H, \qquad \beta = \eta(1+\chi)/2H, \\ \varkappa &= \eta\left[\left(\chi - \frac{a-1}{a+1}\right)\left(\frac{a+1}{a-1} - \chi\right)\right]^{\frac{1}{2}}/2H, \\ \omega &= \frac{c_1}{H(a^2-1)^{\frac{1}{2}}}\eta\chi^{\frac{1}{2}} \end{aligned} \tag{11}$$

with the signs of the radicals chosen so that $\varkappa$ and ω are nonnegative when they are real.

As a result of well-known properties of the branches, which are recounted in [5], (10) gives a continuous one-to-one mapping of the real positive $\varkappa$-axis, which is the integration path in (6), onto the complex χ-plane for each of the branches $\omega_n(\varkappa)$, $n = 0, 1, 2, \ldots$. Specifically, this mapping is the integration path C shown in Fig. 2 for the symmetrical and asymmetrical branches $\omega_n(\varkappa)$, $n = 1, 2, 3, \ldots$. In this figure and in the subsequent work, Re( ) and Im( ) are used to denote the real and imaginary parts, respectively,

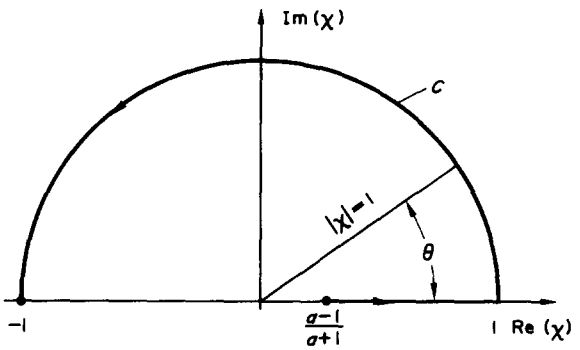

FIG. 2. Integration path C.

of a complex quantity. The point $\chi = (a-1)/(a+1)$ is the mapping of $\varkappa = 0$, $\chi = 1$ is the mapping of points where $\omega_n(\varkappa)/\varkappa = c_1$ and $\chi = -1$ is the mapping of $\varkappa = +\infty$ where $\omega_n(\varkappa)/\varkappa = c_2$. In fact, all branches in "the dilatational sector" of the $\varkappa, \omega$-plane, defined by

$$0 \leq \varkappa \leq \omega/c_1, \tag{12}$$

map onto $(a-1)/(a+1) \leq \chi \leq 1$ and all branches in "the equivoluminal sector", defined by

$$\omega/c_1 \leq \varkappa \leq \omega/c_2, \tag{13}$$

map onto $\chi = e^{i\theta}$, $0 \leq \theta \leq \pi$. On the lowest symmetrical branch $\omega_0(\varkappa)$, $0 \leq \varkappa \leq \omega_0(\varkappa)/c_2$ maps onto $\chi = e^{i\theta}$, $\theta_0 \leq \theta \leq \pi$, where

$$\chi_0 = e^{i\theta_0} = 1-2v^2+2iv(1-v^2)^{\frac{1}{2}} \tag{14}$$

with $\theta_0 = \cos^{-1}(1-2v^2)$ satisfying $0 < \theta_0 < \pi/2$. Also, $\omega_0(\varkappa)/c_2 \leq \varkappa \leq \infty$ maps onto $-1 \leq \chi \leq \chi_R$ where χ_R satisfies $-1 < \chi_R < 0$ and the phase velocity $\omega/\varkappa$ is equal to the Rayleigh surface wave velocity at this point by (11). Similarly, on the lowest asymmetrical branch $\omega_0(\varkappa)$, $0 \leq \varkappa \leq \infty$ maps onto $0 \geq \chi \geq \chi_R$. Thus, integration paths in the χ-plane are specified for all branches.

Under this change of variables, the functions defined by (8) become

$$F_{(\pm)} = \frac{1}{2H^2}\chi\eta^2 G(\chi, v)[\sin(\eta) \pm R(\chi, v)\sin(\chi\eta)] \tag{15}$$

where

$$R(\chi, v) = \frac{(1+\chi)^3-8(1-v)(1+v\chi)\chi}{\chi[(1+\chi)^3-8(1-v)(v+\chi)\chi]} = \frac{(\omega^2/c_2^2-2\varkappa^2)^2-4\varkappa^2\alpha\beta}{(\omega^2/c_2^2-2\varkappa^2)^2+4\varkappa^2\alpha\beta}, \tag{16a}$$

$$G(\chi, v) = (1+\chi)^3-8(1-v)(v+\chi)\chi = 2H^4[(\omega^2/c_2^2-2\varkappa^2)^2+4\varkappa^2\alpha\beta]/\chi\eta^4. \tag{16b}$$

In terms of $\varkappa$ and ω, $\chi\eta^4 G(\chi, v)/2H^4\varkappa^4$ is a function of the phase velocity whose only zero for $0 \leq \varkappa \leq \infty$ is the Rayleigh surface wave velocity. By (10) this zero maps onto χ_R, which is a simple pole of $R(\chi, v)$. $R(\chi, v)$ is the familiar reflection coefficient and $R(e^{i\theta}, v) = e^{i\gamma(\theta,v)}$ on $\chi = e^{i\theta}$ with $\gamma(\theta, v)$ given by (52) in the Appendix.

The Rayleigh–Lamb frequency equation then becomes

$$\sin(\eta) \pm R(\chi, v)\sin(\chi\eta) = 0 \tag{17}$$

with the plus and minus signs corresponding to symmetrical and asymmetrical waves, respectively, with respect to the midplane of the plate with these waves resulting from the

symmetrical and asymmetrical decomposition of the loading (5). The branches of the frequency equation are now taken as the functions $\eta(\chi)$ which satisfy (17) with $\eta_n(\chi)$, $n = 0, 1, 2\ldots$, denoting the mapping of the branches $\omega_n(\varkappa)$, $n = 0, 1, 2, \ldots$, by (10).

Other expressions such as

$$\frac{\mathrm{d}\varkappa}{\mathrm{d}\chi}\Big/\left.\frac{\partial F_{(\pm)}}{\partial\omega}\right|_{F_{(\pm)}=0}$$

are required in terms of χ and η; however, they are not listed here.

The modal solution (6), in the variables χ and η, is

$$\begin{aligned} u(x_1, x_3, t) &= \frac{c_1 I}{4\pi H\mu(a^2-1)^{\frac{1}{4}}}\sum_{n=0}^{\infty}(u_{n(+)}+u_{n(-)}),\\ w(x_1, x_3, t) &= \frac{c_1 I}{4\pi H\mu(a^2-1)^{\frac{1}{4}}}\sum_{n=0}^{\infty}(w_{n(+)}-w_{n(-)}) \end{aligned} \tag{18}$$

where

$$\begin{aligned} u_{n(\pm)} &= \int_C \left.\frac{(1-\chi^2)\sin(\varkappa x_1)\sin(\omega t)\tilde{u}_{(\pm)}}{\chi^{\frac{1}{2}}G(\chi, \nu)[\cos(\eta) \pm \chi R(\chi, \nu)\cos(\chi\eta)]}\right|_{\eta=\eta_n(\chi)} \mathrm{d}\chi,\\ w_{n(\pm)} &= \int_C \left.\frac{(1-\chi)^2(1+\chi)\cos(\varkappa x_1)\sin(\omega t)\tilde{w}_{(\pm)}}{\chi^{\frac{1}{2}}G(\chi, \nu)\left[\left(\chi-\frac{a-1}{a+1}\right)\left(\frac{a+1}{a-1}-\chi\right)\right]^{\frac{1}{4}}[\cos(\eta) \pm \chi R(\chi, \nu)\cos(\chi\eta)]}\right|_{\eta=\eta_n(\chi)} \mathrm{d}\chi. \end{aligned} \tag{19}$$

The integration path C is shown in Fig. 2 for $n = 1, 2, 3\ldots$ and it takes the forms just described for the lowest symmetrical and asymmetrical branches $n = 0$. $\varkappa$ and ω are now functions of χ and η given by (11). The factors $\cos(\eta)\pm\chi R(\chi, \nu)\cos(\chi\eta)$ in (19) result from the derivative $\mathrm{d}\varkappa/\mathrm{d}\chi$, which is required for the change of variables, and they replace the rather complicated functions

$$\left.\frac{\partial F_{(\pm)}}{\partial\omega}\right|_{F_{(\pm)}=0}$$

in (6). The functions $\tilde{u}_{(\pm)}$ and $\tilde{w}_{(\pm)}$ become

$$\begin{aligned} \tilde{u}_{(+)} &= [\chi^2-2(1-2\nu)\chi+1]\cos[\eta(1-\chi)x_3/2H]\sin[\tfrac{1}{2}\eta(1+\chi)]\\ &\quad -(1-\chi^2)\sin[\tfrac{1}{2}\eta(1-\chi)]\cos[\eta(1+\chi)x_3/2H],\\ \tilde{u}_{(-)} &= [\chi^2-2(1-2\nu)\chi+1]\sin[\eta(1-\chi)x_3/2H]\cos[\tfrac{1}{2}\eta(1+\chi)]\\ &\quad -(1-\chi^2)\cos[\tfrac{1}{2}\eta(1-\chi)]\sin[\eta(1+\chi)x_3/2H],\\ \tilde{w}_{(+)} &= [\chi^2-2(1-2\nu)\chi+1]\sin[\eta(1-\chi)x_3/2H]\sin[\tfrac{1}{2}\eta(1+\chi)]\\ &\quad +\left(\chi-\frac{a-1}{a+1}\right)\left(\frac{a+1}{a-1}-\chi\right)\sin[\tfrac{1}{2}\eta(1-\chi)]\sin[\eta(1+\chi)x_3/2H],\\ \tilde{w}_{(-)} &= [\chi^2-2(1-2\nu)\chi+1]\cos[\eta(1-\chi)x_3/2H]\cos[\tfrac{1}{2}\eta(1+\chi)]\\ &\quad +\left(\chi-\frac{a-1}{a+1}\right)\left(\frac{a+1}{a-1}-\chi\right)\cos[\tfrac{1}{2}\eta(1-\chi)]\cos[\eta(1+\chi)x_3/2H]. \end{aligned} \tag{20}$$

This form of the modal solution actually offers no computational advantages over (6). The frequency spectrum, now made up of the branches $\eta_n(\chi)$, $n = 0, 1, 2 \ldots$, is well understood; however, the complexity of much of the high-frequency portion of the spectrum is not at all conducive to integration over the branches. Hence, any advantage from (18) must be obtained by manipulation of the integrals such as deforming the paths of integration, using analytic continuations, expanding functions, etc. It is by these methods that the modal solution (18) is evaluated for the high-frequency response of the plate.

4. BRANCHES OF THE FREQUENCY EQUATION

The form of the branches and certain of their properties are listed for use in evaluating the modal solution (18) with emphasis on the high-frequency response. All of the branches $\eta(\chi)$ which map into the sectors (12) and (13) by (11) have been studied by Mindlin [2] and they are reconsidered here only to show their form in the χ and η variables. The branches are thoroughly investigated in [5].

Some simple results in [5] are sufficient to assure that a complete understanding of the branches can be gained by studying the branches only on the half disk

$$|\chi| \leq 1, \qquad \mathrm{Im}(\chi) \geq 0. \tag{21}$$

Attention is restricted to this half disk with emphasis on its boundary where the branches are relatively simple and where the integration path C in (19) is found.

The additional restriction of $\mathrm{Re}(\eta) \geq 0$ is imposed without loss of generality since $-\eta(\chi)$ obviously satisfies the same frequency equation (17) as does $\eta(\chi)$.

The real branches on $-1 \leq \chi \leq 1$ are sketched in Fig. 3 along with a grid made up of the hyperbolas $\eta = p\pi/(1-\chi)$ and $\eta = q\pi/(1+\chi)$ for $p, q = 1, 2, 3, \ldots$. This grid was also used by Mindlin [2] as an aid to sketching and bounding the branches. These branches are easily sketched or calculated from various forms of the frequency equation (17).

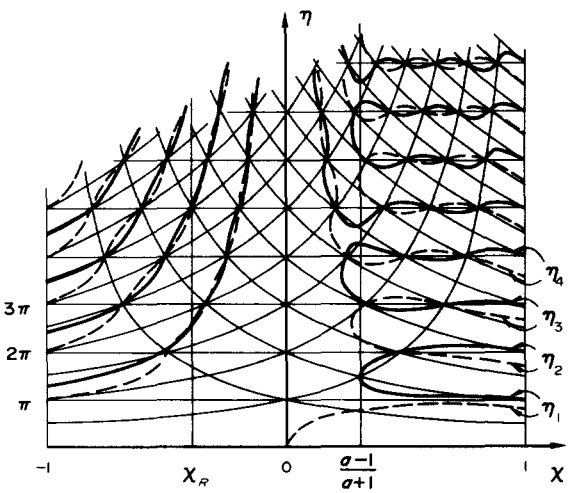

FIG. 3. Real branches on $-1 \leq \chi \leq 1$: solid lines, symmetrical branches; dashed lines, asymmetrical branches.

The real branches on $(a-1)/(a+1) \leq \chi \leq 1$ map into the sector (12) by (11) and those on $0 < \chi \leq (a-1)/(a+1)$ map into the $\varkappa, \omega$-space with $\varkappa$ pure imaginary and ω real. Both of these sets of branches have been studied by Mindlin [2]. As noted from Fig. 3, the latter set of branches are multi-valued with vertical tangents. The branches on $-1 \leq \chi < 0$ are single-valued; however, they map into the $\varkappa, \omega$-space with both $\varkappa$ and ω pure imaginary. These branches, which apparently have not been investigated before, are not important to this work except to illuminate important branches on $|\chi| = 1$ which continue onto these through $\chi = -1$.

Branches with η complex occur on $-1 \leq \chi < (a-1)/(a+1)$, but not on $(a-1)/(a+1) \leq \chi < 1$, and these are investigated in [5]. However, they are not considered here except to state that the lowest asymmetrical branch $\eta_0(\chi)$ is a complex branch occurring on $\chi_R \leq \chi \leq 0$ as is a portion of the lowest symmetrical branch $\eta_0(\chi)$ on $-1 \leq \chi \leq \chi_R$.

It is shown very simply in [5] that, on $\chi = e^{i\theta}$, η must take one of the two forms

$$\eta(e^{i\theta}) = |\eta| e^{-i\theta/2}, \tag{22a}$$

$$\eta(e^{i\theta}) = i|\eta| e^{-i\theta/2}. \tag{22b}$$

Branches of the form (22a) are called the equivoluminal branches and they are sketched on $\chi = e^{i\theta}, 0 \leq \theta \leq \pi$, in Fig. 4 where they are shown as continuations of the real branches on the Re(χ)-axis through the point $\chi = 1(\theta = 0)$. These branches map into sector (13) by (11). Similarly, branches of the form (22b), called the dilatational branches, are sketched on the same interval in Fig. 5 where they are shown as continuations of the real branches on the Re(χ)-axis through $\chi = -1$ ($\theta = \pi$); however, they map into the $\varkappa, \omega$-space with both $\varkappa$ and ω pure imaginary. In addition, the hyperbolas $\eta = q\pi/(1+\chi)$ and $\eta = p\pi/(1-\chi)$ are also shown in these figures where they become the bounds $|\eta| = \frac{1}{2}q\pi \sec(\theta/2)$ and $|\eta| = \frac{1}{2}p\pi \csc(\theta/2)$ for the equivoluminal and dilatational branches, respectively. The point $\chi_{-1} = e^{i\theta_{-1}}$ with $\theta_{-1} = \cos^{-1}(1-2\nu)$ is indicated in these figures, and it is the mapping of the Lamé point where $\omega/\varkappa = \sqrt{(2)}c_2$.

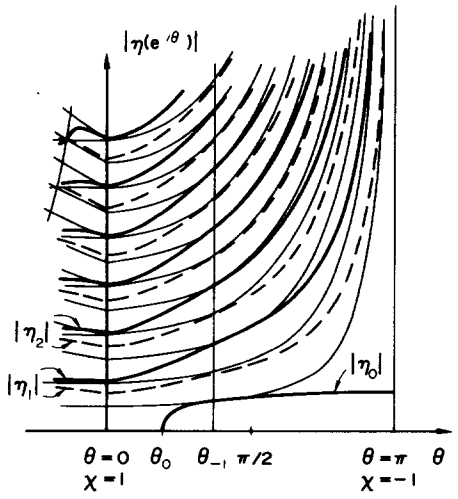

FIG. 4. Equivoluminal branches on $\chi = e^{i\theta}, 0 \leq \theta \leq \pi$: solid lines, symmetrical branches; dashed lines, asymmetrical branches.

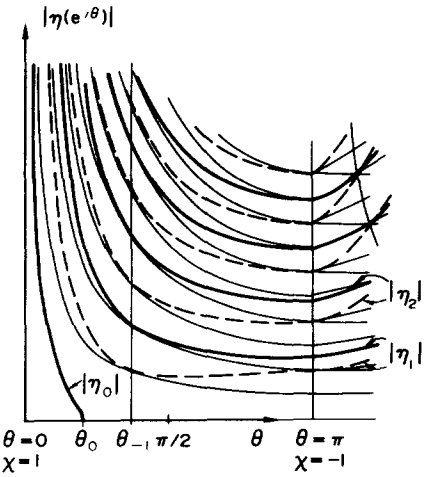

FIG. 5. Dilatational branches on $\chi = e^{i\theta}$. $0 \leq \theta \leq \pi$: solid lines, symmetrical branches; dashed lines, asymmetrical branches.

Analyticity of the branches

Perhaps the most important property of the branches of the frequency equation is that they are analytic functions of χ except at certain singular points in the complex χ-plane. This makes available the Cauchy–Goursat theorem for integration in the χ-plane over the branches and the use of analytic continuations of the branches.

Analyticity of the branches is a result of the existence of the derivative $d\eta/d\chi$. This is considered in detail in [5].

The branches are not analytic at points where they are unbounded such as the singularities seen in Figs. 3–5. By examining the frequency equation under the condition that $\eta \to \infty$, it can be shown that the four points $\chi = 1, 0, \chi_R$ and -1 are the only points where η can be unbounded on the half disk (21). All of the complex branches on the Re(χ)-axis are unbounded at χ_R.

The points where the derivative $d\eta/d\chi$ fails to exist but η is bounded are the most numerous and interesting singularities. These can be shown to be square root branch points, with the result that they are common to just two branches. By means of an investigation, which is described in [5], these branch points are found in three sets on the half disk (21) which are distinguished by their location and by the branches to which they are common.

The first set of branch points occur on $0 \leq \chi \leq (a-1)/(a+1)$ and they are just the vertical tangent points which are seen in Fig. 3. These include a branch point at $\chi = 0$ which is common to the real asymmetrical branch η_1 on $0 \leq \chi \leq 1$ and the pure imaginary asymmetrical branch η_0 on $\chi_R \leq \chi \leq 0$. An additional branch point, which can be included in this set, occurs at $\chi = \chi_0$ given by (14). It is common to the lowest symmetrical equivoluminal branch $\eta_0(e^{i\theta}) = |\eta_0| e^{-i\theta/2}$ and the lowest symmetrical dilatational branch $\eta_0(e^{i\theta}) = i|\eta_0| e^{-i\theta/2}$ as seen in Figs. 4 and 5.

The other two sets of branch points are interior to and not on the boundary of the half disk. The second set occurs approximately adjacent to the line segment $(a-1)/(a+1) \leq \chi < 1$ with the branch points being common to neighboring pairs of real symmetrical

or asymmetrical branches on $(a-1)/(a+1) \leq \chi \leq 1$. For example, the branch $\eta_n(\chi)$ shares branch points from the second set with the branches $\eta_{n-1}(\chi)$ and $\eta_{n+1}(\chi)$ but with no others. An obvious result is that an analytic continuation can be made from one of these branches onto either its upper or lower neighboring branch by taking a continuation path which loops around a common branch point.

Similarly, the third set of branch points occurs adjacent to the line segment $-1 < \chi < 0$ with the branch points being common to pairs consisting of a real branch and a complex branch with $\mathrm{Im}(\eta) > 0$ on $-1 \leq \chi \leq 0$.

This knowledge of singularities of the branches is used extensively for analytic continuations of the branches which, in turn, are used to manipulate and rearrange integrals over the branches.

Analytic continuations of the branches

Analytic continuations of the branches are developed to transform a usual modal representation of the response of the plate into a form which readily yields high-frequency information. The continuations which are useful for this purpose continue around branch points from the second set described in the preceding. This set of branch points is shown schematically in Fig. 6. The branch points are indicated by dots on vertical lines connecting neighboring real branches on $(a-1)/(a+1) \leq \chi \leq 1$ which share the branch points. Also shown in Fig. 6 are some of the first set of branch points $0 \leq \chi \leq (a-1)/(a+1)$. However, these are not involved in the proposed continuations.

The continuations of interest here begin on a branch at $\chi = (a-1)/(a+1)$ and proceed along the $\mathrm{Re}(\chi)$-axis in the positive direction. Each of the branch points from the second set which is common to the branch in question is circled as shown in Fig. 7.

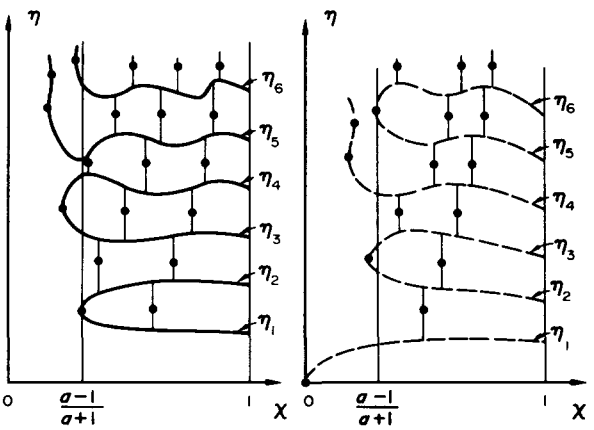

FIG. 6. Schematic representation of branch points: solid lines, symmetrical branches; dashed lines, asymmetrical branches.

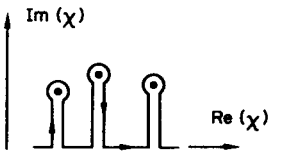

FIG. 7. Path of continuation about branch points.

Two basic types of analytic continuations result from this procedure. These are distinguished by the type of branch they ultimately lead to if the continuation proceeds toward $\chi = 1$ and onto $\chi = e^{i\theta}$, $0 \leq \theta \leq \pi$. This is illustrated by using Fig. 6 to describe example continuations.

The first continuation begins on the symmetrical branch η_6 at $(a-1)/(a+1)$ and continues around every branch point from the second set encountered adjacent to the Re(χ)-axis between $(a-1)/(a+1)$ and $\chi = 1$ and stair steps down successively on the branches η_5, η_4 and finally on η_3, which continues onto the symmetrical equivoluminal branch $\eta_3(e^{i\theta}) = |\eta_3| e^{-i\theta/2}$ on $\chi = e^{i\theta}$, $0 \leq \theta < \pi$. This is an example of an equivoluminal continuation.

The other type of continuation is illustrated by beginning on the asymmetrical branch η_1 at $(a-1)/(a+1)$ in Fig. 6 and continuing around every branch point from the second set encountered adjacent to $(a-1)/(a+1) \leq \chi < 1$. This continuation stair steps up successively on the branches η_2, η_3, η_4, etc. An infinite number of branch points are encountered reflecting the fact that $\chi = 1$ is a limit point of the second set of branch points. Ultimately, the continuation leads to the asymmetrical dilatational branch $\eta_1(e^{i\theta}) = i|\eta_1| e^{-i\theta/2}$ on $\chi = e^{i\theta}$, $0 < \theta \leq \pi$. This is verified by using an approximation to show that this is the only branch available for this continuation to lead to. This is an example of a dilatational continuation.

An infinite number of each of these types of continuations exists on the symmetrical and asymmetrical branches.

Series representations for the branches

Detailed knowledge about the individual branches of the frequency equation is not sufficient to allow even a good approximate evaluation of the modal solution (18). In particular, the high-frequency response requires an accurate, integrable representation for all of the branches for large values of the frequency ω. From (11) this means that representations of the branches $\eta(\chi)$ are required in a neighborhood of the points where η is unbounded. The points $\chi = -1$ and $\chi = 1$ are especially important in this respect since they are the only points where the phase velocity $\omega/\varkappa$ approaches the equivoluminal and dilatational body wave velocities with $\varkappa$ and ω unbounded. For this reason, series representations for the branches based on these two points are described.

The series representation

$$\eta_n(\chi) = E_n^{(0)}(\chi) + \sum_{j=1}^{\infty} E^{(j)}(\chi) \exp[-ij(1-\chi)E_n^{(0)}(\chi)] \tag{23}$$

is for the symmetrical equivoluminal branches $n = 0, 1, 2, \ldots$. The derivation of this series is described in [5], and the coefficients $E_n^{(0)}(\chi)$ and the first three of $E^{(j)}(\chi)$ are given by

$$E_n^{(0)}(\chi) = \frac{2n\pi - i \log[R(\chi, v)]}{1+\chi},$$

$$E^{(1)}(\chi) = \frac{i(R^2-1)}{R(1+\chi)},$$

$$E^{(2)}(\chi) = -\frac{i(R^2-1)}{R^2(1+\chi)}\left[\frac{1}{2}(R^2+1)-(1-\chi)\frac{R^2-1}{1+\chi}\right],$$

$$E^{(3)}(\chi) = \frac{i(R^2-1)}{R^3(1+\chi)}\left[\frac{1}{3}(R^4+R^2+1)-\frac{3}{2}(1-\chi)\frac{R^2-1}{1+\chi}+\frac{3}{2}(1-\chi)^2\frac{(R^2-1)^2}{(1+\chi)^2}\right],$$

$\log[R(\chi, v)]$ is defined by requiring $\log[R(e^{i\theta}, v)] = i\gamma(\theta, v)$ when $\chi = e^{i\theta}$, $0 \le \theta \le \pi$.

The series respresentation for the asymmetrical equivoluminal branches $n = 1, 2, 3, \ldots$ is obtained by simply replacing $R = R(\chi, v)$ with $-R$ in (23). This is equivalent to replacing $E_n^{(0)}(\chi)$ with $E_{n-\frac{1}{2}}^{(0)}(\chi)$ and $E^{(j)}(\chi)$ with $(-1)^j E^{(j)}(\chi)$.

Similarly, as is shown in [5], the series representations for the dilatational branches can be obtained from (23). As a result,

$$\eta_m(\chi) = D_m^{(0)}(\chi) + \sum_{k=1}^{\infty} D^{(k)}(\chi)\exp[ik(1+\chi)D_m^{(0)}(\chi)] \tag{24}$$

is for the symmetrical dilatational branches $m = 0, 1, 2 \ldots$ where $D_m^{(0)}(\chi) = -E_m^{(0)}(-1/\chi, -1/R)/\chi$ with $\log(-1/R) = -\log(R) + i\pi$ and $D^{(k)}(\chi) = -E^{(k)}(-1/\chi, -1/R)/\chi$. For these coefficients, $E_m^{(0)}(\chi, R) \equiv E_m^{(0)}(\chi)$ is written as an explicit function of R, and likewise for $E^{(k)}(\chi)$.

Likewise, the series representation for the asymmetrical dilatational branches $m = 1, 2, 3, \ldots$ is obtained by replacing $D_m^{(0)}(\chi)$ with $D_{m-\frac{1}{2}}^{(0)}(\chi)$ and $D^{(k)}(\chi)$ with $(-1)^k D^{(k)}(\chi)$ in (24).

The results of an investigation on the convergence of these series, which is much too lengthy to include here, are listed. Only certain regions of interest in the χ-plane were examined to determine whether or not they are interior to the region of convergence rather than to try to determine the exact form of the region of convergence for each series.

With the exception of the lowest symmetrical equivoluminal and dilatational branches, the series representations for all of the branches converge uniformly with respect to $\chi = e^{i\theta}$ on any closed segment interior to $0 < \theta < \pi$ with the point $\theta = \pi$ included for the equivoluminal branches and $\theta = 0$ included for the dilatational branches. The series for the lowest symmetrical equivoluminal branch, $n = 0$ in (23), converges uniformly with respect to $\chi = e^{i\theta}$ on any closed segment interior to $\theta_0 < \theta \le \pi$ with θ_0 defined by (14). Likewise, the series for the lowest symmetrical dilatational branch, $m = 0$ in (24), converges uniformly with respect to $\chi = e^{i\theta}$ on any closed segment interior to $0 \le \theta < \theta_0$. It is recalled that these two branches share a branch point at $\chi_0 = e^{i\theta_0}$.

In addition to $|\chi| = 1$, there is another path in the χ-plane on which $|R(\chi, v)| = 1$ and it is not an overwhelming task to investigate the convergence of these series. On the half disk (21) such a path connects the points $(a-1)/(a+1)$ and χ_{-1} defined following (22b). The path actually remains interior to the quarter disk $\mathrm{Re}(\chi) > 0$, $\mathrm{Im}(\chi) \ge 0$ and $|\chi| \le 1$. The fact that $|R(\chi, v)| = 1$ on this path simplifies the calculations much as it does on $\chi = e^{i\theta}$, $0 \le \theta \le \pi$; however, the most important motivation for considering convergence here is that integration paths in the modal solution are conveniently deformed onto this path. None of the series representations for the branches converge on all of this path, however, as the branch number n or m increases the series representations converge uniformly with respect to χ on a larger and larger closed segment of this path which includes the end point χ_{-1} and approaches the end point $(a-1)/(a+1)$. This result is precisely that which is required for applications to the high-frequency response of the plate since the upper

branches, as n and m become unbounded, are necessary to represent the possibly discontinuous wave fronts.

5. THE MODAL SOLUTION ON THE EQUIVOLUMINAL AND DILATATIONAL BRANCHES

The modal solution (18), excepting the lowest symmetrical and asymmetrical modes $n = 0$, is shown to be equivalent to a more convenient form consisting of sums of integrals over the equivoluminal and dilatational branches.

Existence of the integrals over the contemplated paths of integration requires writing the parts of the integrals (19) resulting from the dilatational potential ϕ by (2) in the form

$$\operatorname{Im}\left[\int_C F_\phi(\chi, \eta, x_3) \sin(\omega t)\, e^{i\varkappa x_1}\Big|_{\eta=\eta_n(\chi)} d\chi\right] \tag{25}$$

and the parts resulting from the equivoluminal potential ψ in the form

$$\operatorname{Im}\left[\int_C F_\psi(\chi, \eta, x_3)\begin{bmatrix}\sin(\varkappa x_1)\\ \cos(\varkappa x_1)\end{bmatrix} e^{i\omega t}\Big|_{\eta=\eta_n(\chi)} d\chi\right]. \tag{26}$$

The bracketed term indicates that either $\sin(\varkappa x_1)$ or $\cos(\varkappa x_1)$ occur in the integrands as in (19). These forms are constructed for use only on the right half of the plate, $x_1 \geq 0$.

From these, the equivalent form of either the symmetrical or asymmetrical part of the modal solution (18) is

$$\begin{aligned}\sum_{n=1}^{\infty} \operatorname{Im}\left\{\int_{C_E} [F_\phi(\chi, \eta, x_3) \sin(\omega t)\, e^{i\varkappa x_1} + F_\psi(\chi, \eta, x_3)\begin{bmatrix}\sin(\varkappa x_1)\\ \cos(\varkappa x_1)\end{bmatrix} e^{i\omega t}]\Big|_{\eta=\eta_n(\chi)} d\chi\right\}\\ + \sum_{m=0,1}^{\infty} \operatorname{Im}\left\{\int_{C_D} [F_\phi(\chi, \eta, x_3) \sin(\omega t)\, e^{i\varkappa x_1} + F_\psi(\chi, \eta, x_3)\begin{bmatrix}\sin(\varkappa x_1)\\ \cos(\varkappa x_1)\end{bmatrix} e^{i\omega t}]\Big|_{\eta=\eta_m(\chi)} d\chi\right\}.\end{aligned} \tag{27}$$

The justification of the equivalence of (27) and the modal solution (18) is not trivial and that will be discussed shortly. In the first sum of integrals, $\eta_n(\chi)$, $n = 1, 2, 3, \ldots$, are the symmetrical or asymmetrical equivoluminal branches and their analytic continuations. In the second sum of integrals, $\eta_m(\chi)$ are the symmetrical dilatational branches $m = 0, 1, 2, \ldots$ and their analytic continuations or the asymmetrical dilatational branches $m = 1, 2, 3, \ldots$ and their analytic continuations with the sum from $m = 0$ for the symmetrical part and from $m = 1$ for the asymmetrical part.

The integration path C_E, shown in Fig. 8, goes from the point $(a-1)/(a+1)$ to χ_{-1} on the curve on which $|R(\chi, v)| = 1$, which was just discussed. This is done so that all of the branch points in the second set which are common to the equivoluminal branch in question are to the right of this portion of C_E and those belonging to the third set are to the left. If this is not possible due to the location of some of these branch points, small indentions are made so as to leave these branch points on the proper side of the path. The remainder of C_E is on $|\chi| = 1$ as shown. Similarly, the integration path C_D, also shown in Fig. 8, goes from $(a-1)/(a+1)$ to χ_{-1} on the same path with the same comments holding for the branch points common to the dilatational branch in question. From χ_{-1}, C_D continues toward $\chi = 1$ on $|\chi| = 1$ with a small indention about $\chi = 1$ included because

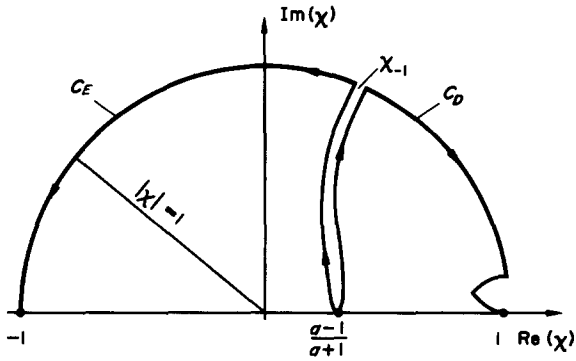

FIG. 8. Integration paths C_E and C_D.

the integrals in (27) fail to exist for certain values of x_1, x_3 and t as $\theta \to 0$ on $\chi = e^{i\theta}$, $0 \leq \theta \leq \pi$. This indention passes above all of the branch points from the second set and, yet, approaches $\chi = 1$ tangent to the Re(χ)-axis. This is possible since this infinite set of branch points is bounded by a curve which is also tangent to the Re(χ)-axis at $\chi = 1$.

The equivalence of the forms (18) and (27) of the modal solution is not shown rigorously since it involves rearranging infinite series which do not converge at the singular wave fronts. However, (27) is shown to involve precisely the same integrals over the same branches as does (18).

For each equivoluminal branch $\eta_n(\chi)$, the integration path C_E is deformed so that it goes from $(a-1)/(a+1)$ to $\chi = 1$ on the Re(χ)-axis with indentions, as shown in Fig. 7, for the branch points of $\eta_n(\chi)$ from the second set. The deformed path then goes from $\chi = 1$ to $\chi = -1$ on $\chi = e^{i\theta}$, $0 \leq \theta \leq \pi$. Likewise, for each dilatational branch $\eta_m(\chi)$, the path C_D is deformed onto $(a-1)/(a+1) \leq \chi \leq 1$ with indentions for the branch points of $\eta_m(\chi)$ from the second set. The Cauchy–Goursat theorem insures that these deformations do not change the values of the integrals.

The representation (27) is then equivalent to sums of integrals over all equivoluminal and dilatational continuations of the branches $\eta_n(\chi)$, $n = 1, 2, 3, \ldots$, with the equivoluminal continuations extending from $(a-1)/(a+1)$ to $\chi = 1$ and then to $\chi = -1$ on $\chi = e^{i\theta}$, $0 \leq \theta \leq \pi$, and the dilatational continuations extending from $(a-1)/(a+1)$ to $\chi = 1$. Hence, (27), with C_E and C_D deformed, certainly involves integrals over exactly the same equivoluminal branches on $\chi = e^{i\theta}, 0 \leq \theta \leq \pi$, as does (18). Referring to Fig. 6 and to the description of the equivoluminal and dilatational continuations from $(a-1)/(a+1)$ to $\chi = 1$, it is seen that (27), with C_E and C_D deformed, covers every portion of every real branch $\eta_n(\chi), n = 1, 2, 3, \ldots$, on $(a-1)/(a+1) \leq \chi \leq 1$. Thus, the same branches have been covered by this integration as in (18).

Only the integrals on the indentions about the branch points remain. Every branch point belonging to the second set is easily seen, from Fig. 6, to be involved just twice in these integrals—once on an equivoluminal continuation and once on a dilatational continuation of the branches. It is then a simple matter to show that the two branch line integrals about a particular branch point mutually cancel.

As a result, (27) is equivalent to (18) by deformation of integration paths and rearrangement of the series. The sum of the symmetrical and asymmetrical parts of the modal solution, each in the form of (27), plus the lowest symmetrical and asymmetrical modes $n = 0$

from (18) or (6) is taken as the response of the plate to the loading (5) and justification of this form as a solution of the equations of motion, the boundary conditions and the initial conditions requires the same demonstration of convergence as does the original modal solution (6).

This rearrangement to form a new modal solution has the very important effect of uncoupling the equivoluminal and dilatational motion.

6. HIGH-FREQUENCY APPROXIMATION OF THE MODAL SOLUTION

The modal solution (27) is approximated by using the series representations for the branches. The solution then involves a sum of integrals whose integrands possess none of the branch points of the branches which were of concern previously. As a result, the integration paths C_E and C_D are deformed so that the summations over the branch numbers n and m can be carried out leaving the solution

$$u(x_1, x_3, t) \cong \frac{c_1 I}{16\pi H\mu(a^2-1)^{\frac{1}{2}}}(I_{de}+I_{ee}+I_{dd}+I_{ed}). \tag{28}$$

The integrals I_{de}, I_{ee}, I_{dd} and I_{ed} are given by (49a), ..., (49d) and (50) in the Appendix. The detailed derivation of (28) is contained in [5], and an unresolved difficulty concerning singularities arising from zeros of $R(\chi, v)$ is also discussed there. These integrals are written with their subscripts indicating their origin with, for example, I_{de} being the integral resulting from the dilatational potential ϕ with the integration over the equivoluminal branches.

The two lowest modes, resulting from the lowest symmetrical and asymmetrical branches $n = 0$, are not included in (28). In addition to this, the expression is approximate since the series representations for the branches do not converge on the entire integration paths C_E and C_D. However, this is expected to be a very good high-frequency approximation since it is recalled that the regions of convergence include the entire paths C_E and C_D as a limit when the branch numbers n and m approach infinity.

A similar high-frequency approximation for the displacement component $w(x_1, x_3, t)$ can be written by making simple changes in (49a), ..., (49d) and (50) as indicated by (18).

7. THE WAVE FRONTS

For further calculations, the various functions (54) replace χ or θ as the independent variable in the preceding integrals so that $(d\chi/d\Phi)\,d\Phi$ replaces $d\chi$ with Φ representing one of these four functions. The condition for a singular wave front is the simultaneous satisfaction of

$$\Phi = 2m, \qquad \frac{d\Phi}{d\chi} = 0 \tag{29}$$

for any integer m such that $\Phi = 2m$ occurs in the range of integration. The first equation gives the singular points of the generalized functions $\csc[(\pi/2)\Phi]$, $\cot[(\pi/2)\Phi]$ and $\delta(\Phi-2m)$ and the second equation makes $d\chi/d\Phi$, which is now a part of the integrand, singular. Under this condition, the Cauchy principal value integrals and the last sum of integrals in (50) fail to exist causing singularities which are identified as wave fronts.

For $l = 1, 3, 5, 7, d\Phi/d\chi = 0$ is not possible for the range of variables considered here and, hence, only the terms in the integrals containing the functions (54) identified by $l = 2, 4, 6, 8$ contain wave fronts.

Parametric equations for the singular wave fronts are given by (29) for each of the functions in (54). These wave fronts are sketched in Fig. 9 with their origin indicated by the quantities $Q_{pq}^{(e)} = (2p+2q+1\mp1)H/c_2t$ and $Q_{pq}^{(d)} = (2p+2q+1\pm1)H/c_2t$ where the upper signs apply for $l = 2, 4$ and the lower signs for $l = 6, 8$. The equivoluminal fronts, described by $\Phi = \Psi_{lpq}^{(e)}$ in (29), are indicated by $Q_{pq}^{(e)}$ and they are contained in I_{ee}. Likewise, the dilatational fronts, described by $\Phi = \Phi_{lpq}^{(d)}$ in (29), are indicated by $Q_{pq}^{(d)}$ and they are contained in I_{dd}. The figure is at time $t = 6{\cdot}3H/c_2$ for $\nu = 0{\cdot}3$ so that the circular equivoluminal wave $Q_{pq}^{(e)} = 0$ has crossed the plate $c_2t/2H = 3{\cdot}15$ times at $x_1 = 0$ while the circular dilatational wave $Q_{pq}^{(d)} = 0$ has crossed the plate $c_1t/2H \cong 5{\cdot}89$ times. The top sketch in Fig. 9 just shows the thickness $-H \leq x_3 \leq H$ successively repeated so that all wave fronts appear as smooth curves. The geometry is the same as for a layered half space with refractions but no reflections at the junctions. The bottom sketch shows the superposition of these wave fronts as they appear in the plate and this is obtained by folding the top sketch as an accordian at each horizontal line to form a single plate thickness.

The familiar head wave is also shown in Fig. 9. This wave front is singular for the stresses but not for the displacements for the loading (5) and it is contained in I_{ee} in the principal value integrals of (49b) and (50) as well as in the integrals of (50) containing the delta

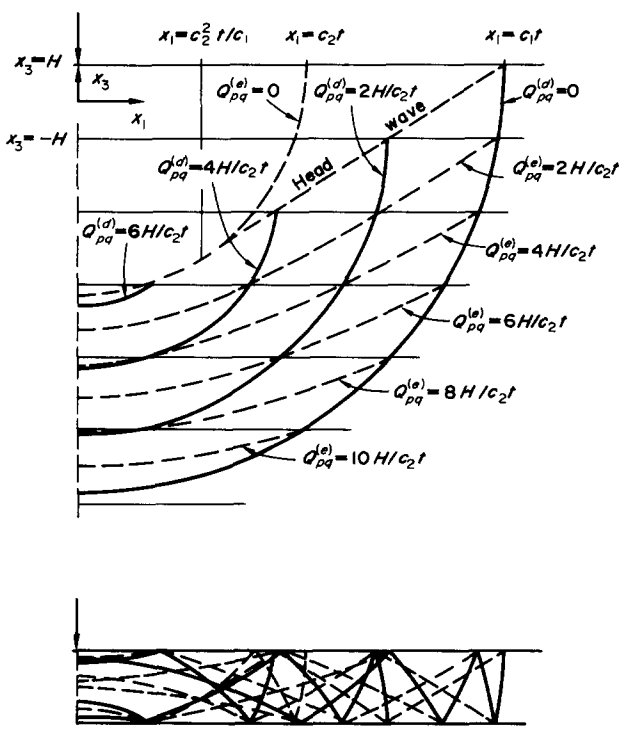

FIG. 9. Wave fronts at $t = 6{\cdot}3H/c_2$ for $\nu = 0{\cdot}3$: solid lines, dilatational fronts; dashed lines, equivoluminal fronts.

functions. This front results entirely from the point $\chi = 1$ or $\theta = 0$ where the integrand vanishes as will be seen in some of the following calculations.

The finite number of parameters $Q_{pq}^{(e)}$ and $Q_{pq}^{(d)}$ required to represent all of the wave fronts in Fig. 9 means that only a finite number of coefficients A_{pq} and A'_{pq} are needed if only the terms in (49b), (49c) and (50) which contain singular wave fronts are of interest. Specifically, A_{pq} for $p+q \leq 5$ and A'_{pq} for $p+q \leq 3$ are needed for the equivoluminal and dilatational fronts, respectively. This, in turn, means that only a finite number of the coefficients $E^{(j)}(\chi)$ and $D^{(k)}(\chi)$ are needed for this purpose.

There are wave fronts, other than those shown in Fig. 9, which are predicted by (29); however, these can be shown to cancel when the integral sums $I_{de}+I_{dd}$ and $I_{ee}+I_{ed}$ in (28) are examined carefully. Thus, if only the wave fronts are of interest in the response, the only function of the terms I_{de} and I_{ed} in (28) is to cancel extraneous wave fronts.

8. SPECIFIC TERMS CONTAINING WAVE FRONTS

Certain parts of the solution (28) are evaluated or approximated to compare with known exact solutions of the Lamb's problem of a line load on a half space and to illustrate how the principal value integrals are to be evaluated.

The last sum of integrals in (50) are the only ones that can be easily evaluated in an algebraic form, which is done by taking advantage of the properties of the delta functions $\delta(\Psi_{l00}^{(e)} - 2m)$. It was found that only the terms $l = 2, 4$ in this sum may contain singular wave fronts and only $l = 2$ contains an unreflected portion of the circular equivoluminal wave front $Q_{pq}^{(e)} = 0$ shown in Fig. 9. This term is treated for a comparison with the half space solution. From (51), $S_{12}+(-1)^m S_{22} = 1+(-1)^m$ and the portion of (28) containing this $l = 2$ term is

$$u(x_1, x_3, t) \cong \frac{c_1 I}{2\pi H\mu(a^2-1)^{\frac{1}{2}}} \sum_{m=-\infty}^{\infty} \int_0^{\pi} \frac{\sin(\theta/2)\sin(\theta)}{|G(e^{i\theta}, \nu)|} \cos[(2m+\tfrac{1}{2})\gamma]\delta(\Psi - 4m)\, d\theta \tag{30}$$

where

$$\Psi = \Psi_{200}^{(e)} = \frac{a}{H(a^2-1)^{\frac{1}{2}}\cos(\theta/2)} \left\{ c_2 t - x_1 \left[1 - \frac{a^2-1}{a^2}\cos^2(\theta/2) \right]^{\frac{1}{2}} \right\} - 1 + x_3/H. \tag{31}$$

The inverse of $\Psi = \Psi(\theta)$ is

$$\cos\left(\frac{\theta_s}{2}\right) = \frac{a}{(a^2-1)^{\frac{1}{2}}} \frac{(H\Psi+H-x_3)c_2 t - (-1)^s x_1[(H\Psi+H-x_3)^2 + x_1^2 - c_2^2 t^2]^{\frac{1}{2}}}{(H\Psi+H-x_3)^2 + x_1^2}, \tag{32}$$

with $s = 1, 2$ denoting the two possible branches. A critical point with $d\theta_s/d\Psi$ unbounded occurs at

$$\Psi = \Psi_c = (c_2^2 t^2 - x_1^2)^{\frac{1}{2}}/H - 1 - x_3/H \tag{33}$$

where

$$\cos\left(\frac{\theta_1}{2}\right) = \cos\left(\frac{\theta_2}{2}\right) = \frac{a}{(a^2-1)^{\frac{1}{2}}}(c_2^2 t^2 - x_1^2)^{\frac{1}{2}}/c_2 t.$$

This point is in the range $0 \le \theta \le \pi$ only if $c_2^2 t/c_1 \le x_1 \le c_2 t$ and it is associated with this portion of the wave front $Q_{pq}^{(e)} = 0$ in Fig. 9.

With

$$\frac{d\theta_s}{d\Psi} = -2\csc\left(\frac{\theta_s}{2}\right)\frac{d}{d\Psi}\left[\cos\left(\frac{\theta_s}{2}\right)\right],$$

where

$$\frac{d}{d\Psi}\left[\cos\left(\frac{\theta_s}{2}\right)\right] = \frac{Ha}{(a^2-1)^{\frac{1}{2}}}\left\{\frac{c_2 t[x_1^2-(H\Psi+H-x_3)^2]}{[(H\Psi+H-x_3)^2+x_1^2]^2}\right.$$

$$\left.-(-1)^s\frac{x_1(H\Psi+H-x_3)[2c_2^2t^2-x_1^2-(H\Psi+H-x_3)^2]}{[(H\Psi+H-x_3)^2+x_1^2]^2[(H\Psi+H-x_3)^2+x_1^2-c_2^2t^2]^{\frac{1}{2}}}\right\}, \tag{34}$$

(30) becomes

$$u(x_1, x_3, t) \cong \frac{-c_1 I}{\pi H\mu(a^2-1)^{\frac{1}{2}}}\sum_{m=-\infty}^{\infty}\left\{\int_{\Psi_c}^{\Psi(0)}\frac{\sin(\theta)}{|G(e^{i\theta}, \nu)|}\cos\left[\left(2m+\frac{1}{2}\right)\gamma\right]\Big|_{\theta=\theta_1(\Psi)}\right.$$

$$\times\,\delta(\Psi-4m)\frac{d}{d\Psi}\left[\cos\left(\frac{\theta_1}{2}\right)\right]d\Psi$$

$$\left.-\int_{\Psi_c}^{\infty}\frac{\sin(\theta)}{|G(e^{i\theta}, \nu)|}\cos\left[\left(2m+\frac{1}{2}\right)\gamma\right]\Big|_{\theta=\theta_2(\Psi)}\delta(\Psi-4m)\frac{d}{d\Psi}\left[\cos\left(\frac{\theta_2}{2}\right)\right]d\Psi\right\}$$

$$= \frac{-c_1 I}{\pi H\mu(a^2-1)^{\frac{1}{2}}}\sum_{m=m_c}^{m_0}\frac{\sin(\theta)}{|G(e^{i\theta}, \nu)|}\cos\left[\left(2m+\frac{1}{2}\right)\gamma\right]\Big|_{\theta=\theta_1(4m)}\frac{d}{d\Psi}\left[\cos\left(\frac{\theta_1(4m)}{2}\right)\right]$$

$$-\sum_{m=m_c}^{\infty}\frac{\sin(\theta)}{|G(e^{i\theta}, \nu)|}\cos\left[\left(2m+\frac{1}{2}\right)\gamma\right]\Big|_{\theta=\theta_2(4m)}\frac{d}{d\Psi}\left[\cos\left(\frac{\theta_2(4m)}{2}\right)\right] \tag{35}$$

for $c_2^2 t/c_1 \le x_1 \le c_2 t$ where

$$\Psi(0) = \frac{1}{H(a^2-1)^{\frac{1}{2}}}(c_1 t - x_1) - 1 + x_3/H \tag{36}$$

results from (31), m_c is defined as the minimum integer such that $4m_c \ge \Psi_c$ and m_0 is the maximum integer such that $4m_0 \le \Psi(0)$.

If x_1 and x_3 are further restricted to the region $c_2^2 t/c_1 \le [c_2^2 t^2-(H-x_3)^2]^{\frac{1}{2}} \le x_1 \le c_2 t$ and $-H \le x_3 \le H$, then $m_c = 0$ and the value $m = m_c = 0$ is easily identified with the unreflected portion of the circular equivoluminal wave front. Retaining only the $m = 0$ term from (35) leaves

$$u(x_1, x_3, t) \cong \frac{-c_1 I}{\pi H\mu(a^2-1)^{\frac{1}{2}}}\left\{\frac{\sin(\theta)}{|G(e^{i\theta}, \nu)|}\cos\left(\frac{\gamma}{2}\right)\Big|_{\theta=\theta_1(0)}\frac{d}{d\Psi}\left[\cos\left(\frac{\theta_1(0)}{2}\right)\right]\right.$$

$$\left.-\frac{\sin(\theta)}{|G(e^{i\theta}, \nu)|}\cos\left(\frac{\gamma}{2}\right)\Big|_{\theta=\theta_2(0)}\frac{d}{d\Psi}\left[\cos\left(\frac{\theta_2(0)}{2}\right)\right]\right\} \tag{37}$$

and, from (32) and (34), this can be written as

$$u(x_1, x_3, t) \cong \frac{F\{x_1, x_3, t, [x_1^2+(H-x_3)^2-c_2^2t^2]^{\frac{1}{2}}\}+F\{x_1, x_3, t, -[x_1^2+(H-x_3)^2-c_2^2t^2]^{\frac{1}{2}}\}}{[x_1^2+(H-x_3)^2-c_2^2t^2]^{\frac{1}{2}}}. \tag{38}$$

The function F exhibits explicit dependence on the radical $[x_1^2+(H-x_3)^2-c_2^2t^2]^{\frac{1}{2}}$ and it is analytic with respect to this radical and nonzero in a neighborhood of and including the point where the radical vanishes.

With some algebra and using the fact that $\cos(\gamma/2)/|G(e^{i\theta}, v)| = \mathrm{Re}[e^{i\theta}/G(e^{i\theta}, v)]$, it can be shown that the first part of (38), containing F with the positive radical, is one half of the exact solution in this region for the Lamb's problem of a half space with the loading on $x_3 = H$ given by (5). This solution is found in a convenient form in the work of Gakenheimer and Miklowitz [6] for a traveling load on a half space by letting the load velocity approach infinity. Furthermore, (38) gives all of the odd powers, $-1, 1, 3, 5, \ldots$, of $[x_1^2+(H-x_3)^2-c_2^2t^2]^{\frac{1}{2}}$ in a wave front expansion as the circular equivoluminal wave front is approached from the region $c_2^2t/c_1 \leq [c_2^2t^2-(H-x_3)^2]^{\frac{1}{2}} \leq x_1 \leq c_2t$. The even powers, $0, 2, 4, \ldots$, are not contained in (38), but these terms, and any of their derivatives, are not singular at the wave front and they are probably contained in other parts of the representation (28).

One half of the head wave response is also contained in the first term of (38), which can be extended to $x_1 \geq c_2t$, and it stems from the term $\sin[\theta_1(0)]$. This term can be shown from (32) to behave like $[c_1t-x_1-(a^2-1)^{\frac{1}{2}}(H-x_3]^{\frac{1}{2}}$ near the unreflected portion of the head wave. The remainder of the unreflected head wave response is contained in the second integrals in (50) and in the first integrals in (49b) and in both cases it is associated with $\Psi_{200}^{(e)} = 0$ occurring at $\chi = 1(\theta = 0)$.

Even order reflections of the circular equivoluminal wave front are contained in (35) with $m = 0$ containing the unreflected portion, as just treated, $m = 1$ containing the second reflection, etc. The odd reflections are contained in terms derived in the same manner from the last sum of integrals in (50) for $l = 4$.

The singular response following this portion of the circular equivoluminal wave front, this being the "two-sided" equivoluminal wave front, is contained in the principal value integrals in (50) for $l = 2, 4$. The remainder of this wave front on $0 \leq x_1 \leq c_2^2t/c_1$, which is "one-sided", is contained in the first sum of integrals in (49b) for $l = 2, 4$ and $p = q = 0$.

As an example of a principal value integral and for another comparison with the known half space solution, the term I_{dd} in (49c), which contains the circular dilatational wave front $Q_{pq}^{(d)} = 0$ in Fig. 9, is considered. $Q_{pq}^{(d)} = 0$ only for $l = 6, 8$ and $p = q = 0$ and the term $l = 8$ contains the unreflected portion of this wave front. From (51),

$$S_{18}\csc\left(\frac{\pi}{2}\Phi\right)+S_{28}\cot\left(\frac{\pi}{2}\Phi\right) = -\cot\left(\frac{\pi}{4}\Phi\right)$$

and, using $A_{00}' = 1$, the portion of (28) containing this $l = 8$ term is

$$u(x_1, x_3, t) \cong \frac{-c_1I}{32\pi H\mu(a^2-1)^{\frac{1}{2}}}P.V.\int_{(a-1)/(a+1)}^{1} \frac{(1+\chi)[\chi^2-2(1-2v)\chi+1]}{\chi^{\frac{1}{2}}G(\chi, v)} \times \exp\left(-\frac{1}{2}\Phi\log R\right)\cot\left(\frac{\pi}{4}\Phi\right)d\chi \tag{39}$$

where

$$\Phi = \Phi_{800}^{(d)} = \frac{x_1}{H(1-\chi)}\left[\left(\chi-\frac{a-1}{a+1}\right)\left(\frac{a+1}{a-1}-\chi\right)\right]^{\frac{1}{2}} - \frac{2c_1 t}{H(a^2-1)^{\frac{1}{2}}(1-\chi)}\chi^{\frac{1}{2}} + 1 - x_3/H. \quad (40)$$

The inverse of $\Phi = \Phi(\chi)$ is most conveniently found by first solving for $(1-\chi)/\chi^{\frac{1}{2}}$ and then for χ with two possible branches $\chi_1(\Phi)$ and $\chi_2(\Phi)$, expected. A critical point, where $d\chi/d\Phi$ is unbounded, occurs with $(a-1)/(a+1) \le \chi \le 1$ if $0 \le x_1 \le c_1 t$ and it is

$$\Phi_c = 1 - x_3/H - (c_1^2 t^2 - x_1^2)^{\frac{1}{2}}/H \quad (41)$$

where

$$\chi_1(\Phi_c) = \chi_2(\Phi_c) = \frac{1}{(a^2-1)c_1^2 t^2}[(c_1^4 t^2/c_2^2 - x_1^2)^{\frac{1}{2}} - (c_1^2 t^2 - x_1^2)^{\frac{1}{2}}]^2. \quad (42)$$

This critical point is associated with the circular dilatational wave front $Q_{pq}^{(d)} = 0$ in Fig. 9.

With Φ as the integration variable, (39) becomes

$$\begin{aligned} u(x_1, x_3, t) &\cong P.V. \int_{(a-1)/(a+1)}^{1} f(\chi) \cot\left(\frac{\pi}{4}\Phi\right) d\chi \\ &= P.V. \int_{\Phi[(a-1)/(a+1)]}^{\Phi_c} f(\chi_1)\frac{d\chi_1}{d\Phi}\cot\left(\frac{\pi}{4}\Phi\right) d\Phi - P.V. \int_{-\infty}^{\Phi_c} f(\chi_2)\frac{d\chi_2}{d\Phi}\cot\left(\frac{\pi}{4}\Phi\right) d\Phi \end{aligned} \quad (43)$$

with $f(\chi) = f(x_1, x_3, t, \chi)$ determined from (39) and $\Phi[(a-1)/(a+1)] = 1 - x_3/H - c_1 t/H$ from (40).

The last integral in (43) and all principal value integrals in (49a), ..., (49d) and (50) which involve an infinite set of singularities should be interpreted as

$$\begin{aligned} P.V. \int_{-\infty}^{\Phi_c} f(\chi_2)\frac{d\chi_2}{d\Phi}\cot\left(\frac{\pi}{4}\Phi\right) d\Phi &= P.V. \int_{4M_c-2}^{\Phi_c} f(\chi_2)\frac{d\chi_2}{d\Phi}\cot\left(\frac{\pi}{4}\Phi\right) d\Phi \\ &\quad + \sum_{m=-M_c}^{\infty} P.V. \int_{-4m-6}^{-4m-2} f(\chi_2)\frac{d\chi_2}{d\Phi}\cot\left(\frac{\pi}{4}\Phi\right) d\Phi \\ &= P.V. \int_{4M_c-2}^{\Phi_c} f(\chi_2)\frac{d\chi_2}{d\Phi}\cot\left(\frac{\pi}{4}\Phi\right) d\Phi \\ &\quad - \frac{4}{\pi}\int_{-\infty}^{4M_c-2} \frac{d}{d\Phi}\left[f(\chi_2)\frac{d\chi_2}{d\Phi}\right] \log\left|\sin\left(\frac{\pi}{4}\Phi\right)\right| d\Phi \end{aligned} \quad (44)$$

where M_c is the integer for which $4M_c - 2 \le \Phi_c \le 4M_c + 2$. Integration by parts was used to reduce the last integral in (44) to an ordinary integral.

The singularity identified as the unreflected portion of the circular dilatational wave front is now contained entirely in the first integral of (43) and in the first integral of (44). This wave front is identified with the singularity of $\cot[(\pi/4)\Phi]$ at $\Phi = 2m = 0$ with $M_c = 0$. Just these two integrals are taken as the approximate response and they are approximated further by evaluating all of the nonsingular parts of the integrands at $\Phi = \Phi_c$ where

$\chi_1 = \chi_2$ to give

$$u(x_1, x_3, t) \cong P.V. \int_{-2}^{\Phi_c} f(\chi_1) \frac{d\chi_1}{d\Phi} \cot\left(\frac{\pi}{4}\Phi\right) d\Phi - P.V. \int_{-2}^{\Phi_c} f(\chi_2) \frac{d\chi_2}{d\Phi} \cot\left(\frac{\pi}{4}\Phi\right) d\Phi$$

$$\cong \frac{Ix_1(c_1^2t^2 - x_1^2)^{\frac{1}{4}}[\chi^2 - 2(1-2\nu)\chi + 1] \exp(-\frac{1}{2}\Phi_c \log R)}{4\pi\mu c_1(a^2-1)t^2 G(\chi, \nu)}\Bigg|_{\chi=\chi_1(\Phi_c)} \tag{45}$$

$$\times P.V. \int_{-2}^{\Phi_c} \frac{\cot\left(\frac{\pi}{4}\Phi\right) d\Phi}{[(H\Phi - H + x_3)^2 + x_1^2 - c_1^2t^2]^{\frac{1}{4}}}.$$

The lower limit of integration $\Phi[(a-1)/(a+1)]$ from (43) has been replaced by -2, but that is of little consequence since only the singular parts of the integrals are of interest here and they stem from the upper limit Φ_c. The radical in the denominator of the integrand results from the derivatives $d\chi_1/d\Phi$ and $d\chi_2/d\Phi$ and it vanishes at $\Phi = \Phi_c$ creating an integrable singularity. However, if $\Phi_c = 0$ this singularity coincides with the singularity $\Phi = 0$ of $\cot[(\pi/4)\Phi]$ and the principal value integral fails to exist. This singular value of the integral is identified with the singular wave front.

The representation (45) is approximated further to get the first term of a wave front expansion by taking $\cot[(\pi/4)\Phi] \cong 4/\pi\Phi$ and assuming that $|\Phi_c| \ll 1$ to get

$$u(x_1, x_3, t) \cong \frac{Ix_1(H - x_3)[\chi^2 - 2(1-2\nu)\chi + 1]}{\sqrt{(2)}\pi\mu c_1^2(a^2-1)t_d^{\frac{1}{2}} G(\chi, \nu)}\Bigg|_{\chi=\chi_1(0)} (t - t_d)^{-\frac{1}{4}} \tag{46}$$

where

$$t_d = [x_1^2 + (H - x_3)^2]^{\frac{1}{2}}/c_1, \tag{47}$$

so that $t = t_d$ makes $\Phi_c = 0$, and

$$\chi_1(0) = \chi_1(\Phi_c)\Big|_{t=t_d} = \frac{\{[(a^2-1)x_1^2 + a^2(H-x_3)^2]^{\frac{1}{2}} - H + x_3\}^2}{(a^2-1)[x_1^2 + (H-x_3)^2]} \tag{48}$$

from (42). (46) agrees exactly with the first term in the wave front expansion obtained from the solution of Lamb's problem of a half space with the loading (5) on $x_3 = H$. Again this solution is contained in the work of Gakenheimer and Miklowitz [6]. This expression is valid for all of the unreflected portion of the wave front $Q_{pq}^{(d)} = 0$ in Fig. 9 and this includes the entire front $0 \leq x_1 \leq c_1 t$ if $c_1 t \leq 2H$.

Analogous to the equivoluminal wave, the second, fourth, sixth, etc., reflections of this dilatational front are also contained in (39) and they are associated with singularities at $\Phi = -4, -8, -12$, etc. As a result, $\exp(-\frac{1}{2}\Phi \log R) = R^2, R^4, R^6$, etc., at these points causing the only major change in the wave front expansion (46). This is consistent with the fact that $R = R(\chi, \nu)$ is the reflection coefficient. The odd order reflections are contained in an integral similar to (39) which results from (49c) with $p = q = 0$ and $l = 6$. Likewise, the first, third, etc., reflections are associated with singularities at $\Phi_{600}^{(d)} = -2, -6$, etc., which produce $\exp(-\frac{1}{2}\Phi_{600}^{(d)} \log R) = R, R^3$, etc., in wave front expansions.

The representation (28), while still quite complex, only involves explicit functions of χ and it offers direct access to the high-frequency response including the wave fronts. This is contrasted with the modal solution (18) or (6) in which details of the high-frequency response are all but invisible. In addition, this representation appears to be considerably more accurate than wave front expansions which diverge rapidly away from the fronts.

REFERENCES

[1] R. L. ROSENFELD and J. MIKLOWITZ, Wave Fronts in Elastic Rods and Plates, *Proc. 4th U.S. natn. Congr. appl. Mech.*, pp. 293–303 (1962).

[2] R. D. MINDLIN, Waves and Vibrations in Isotropic, Elastic Plates, *Structural Mechanics, Proc. 1st Symp. on Naval Struct. Mech.*, pp. 199–232. Pergamon Press (1960).

[3] J. R. LLOYD and J. MIKLOWITZ, On the Use of Double Integral Transforms in the Study of Dispersive Elastic Wave Propagation, *Proc. 4th U.S. natn. Congr. appl. Mech.*, pp. 255–267 (1962).

[4] A. N. HOLDEN, Longitudinal modes of elastic waves in isotropic cylinders and slabs. *Bell Syst. tech. J.* **30**, 956–969 (1951).

[5] P. W. RANDLES, Modal Representations for the High-Frequency Response of Elastic Plates, Ph.D. Thesis, California Institute of Technology (1969).

[6] D. C. GAKENHEIMER and J. MIKLOWITZ, Transient excitation of an elastic half space by a point load traveling on the surface. *J. appl. Mech.* **36**, 505–515 (1969).

APPENDIX

The integrals in (28) are (*P.V.* denotes Cauchy principal values)

$$I_{de} = \sum_{p,q=0}^{\infty}\sum_{l=1}^{8} P.V.\int_{(a-1)/(a+1)}^{1} A_{pq}(\chi,\Phi_l)\frac{(1-\chi)[\chi^2-2(1-2\nu)\chi+1]}{2\chi^{\frac{1}{2}}G(\chi,\nu)}\exp\left(\frac{1}{2}\Phi_{lpq}^{(e)}\log R\right)$$
$$\times\left[S_{1l}\cot\left(\frac{\pi}{2}\Phi_{lpq}^{(e)}\right)+(-1)^pS_{2l}\csc\left(\frac{\pi}{2}\Phi_{lpq}^{(e)}\right)\right]d\chi$$
$$+4Im\left\{\sum_{p,q=0}^{\infty}\sum_{l=1}^{8}\int_0^{\pi}A_{pq}(e^{i\theta},\Phi_l)\frac{\sin(\theta/2)[\cos(\theta)-1+2\nu]}{|G(e^{i\theta},\nu)|}\exp\left[i\frac{\gamma}{2}(\Phi_{lpq}^{(e)}+1)\right]\right. \tag{49a}$$
$$\left.\times\left[S_{1l}+(-1)^pS_{2l}\exp\left(-i\frac{\pi}{2}\Phi_{lpq}^{(e)}\right)\right]\frac{\exp(i\pi\Phi_{lpq}^{(e)})}{1-\exp(i\pi\Phi_{lpq}^{(e)})}d\theta\right\},$$

$$I_{ee} = -\sum_{p,q=0}^{\infty}\sum_{l=1}^{8} P.V.\int_{(a-1)/(a+1)}^{1} A_{pq}(\chi,\Psi_l)\frac{(1-\chi)(1-\chi^2)}{2\chi^{\frac{1}{2}}G(\chi,\nu)}\exp\left(\frac{1}{2}\Psi_{lpq}^{(e)}\log R\right)$$
$$\times\left[S_{1l}\cot\left(\frac{\pi}{2}\Psi_{lpq}^{(e)}\right)+(-1)^pS_{2l}\csc\left(\frac{\pi}{2}\Psi_{lpq}^{(e)}\right)\right]d\chi$$
$$+4\,\mathrm{Re}\left\{\sum_{p,q=0}^{\infty}\sum_{l=1}^{8}\int_0^{\pi}A_{pq}(e^{i\theta},\Psi_l)\frac{\sin(\theta/2)\sin(\theta)}{|G(e^{i\theta},\nu)|}\exp\left[i\frac{\gamma}{2}(\Psi_{lpq}^{(e)}+1)\right]\right. \tag{49b}$$
$$\left.\times\left[S_{1l}+(-1)^pS_{2l}\exp\left(-i\frac{\pi}{2}\Psi_{lpq}^{(e)}\right)\right]\frac{\exp(i\pi\Psi_{lpq}^{(e)})}{1-\exp(i\pi\Psi_{lpq}^{(e)})}d\theta\right\},$$

$$I_{dd} = \sum_{p,q=0}^{\infty}\sum_{l=1}^{8} P.V.\int_{(a-1)/(a+1)}^{1} A'_{pq}(\chi,\Phi_l)\frac{(1+\chi)[\chi^2-2(1-2\nu)\chi+1]}{2\chi^{\frac{1}{2}}G(\chi,\nu)}\exp\left(-\frac{1}{2}\Phi_{lpq}^{(d)}\log R\right)$$
$$\times\left[S_{1l}\csc\left(\frac{\pi}{2}\Phi_{lpq}^{(d)}\right)+(-1)^pS_{2l}\cot\left(\frac{\pi}{2}\Phi_{lpq}^{(d)}\right)\right]d\chi, \tag{49c}$$

$$I_{ed} = -\sum_{p,q=0}^{\infty}\sum_{l=1}^{8} P.V.\int_{(a-1)/(a+1)}^{1} A'_{pq}(\chi,\Psi_l)\frac{(1+\chi)(1-\chi^2)}{2\chi^{\frac{1}{2}}G(\chi,\nu)}\exp\left(-\frac{1}{2}\Psi_{lpq}^{(d)}\log R\right)$$
$$\times\left[S_{1l}\csc\left(\frac{\pi}{2}\Psi_{lpq}^{(d)}\right)+(-1)^pS_{2l}\cot\left(\frac{\pi}{2}\Psi_{lpq}^{(d)}\right)\right]d\chi. \tag{49d}$$

The integrals on $\chi = e^{i\theta}$, $0 \le \theta \le \pi$, in (49b) for I_{ee} must be modified for the terms $p = q = 0$ and $l = 1$–4 since $\Psi^{(e)}_{l00}$ is real. Using $A_{00} = 1$, this sum of integrals is replaced with

$$4\sum_{l=1}^{4}\left\{-\frac{1}{2}S_{1l}\int_0^{\pi}\frac{\sin(\theta/2)\sin(\theta)}{|G(e^{i\theta},v)|}\cos\left[\frac{\gamma}{2}(\Psi^{(e)}_{l00}+1)\right]d\theta-\frac{1}{2}P.V.\int_0^{\pi}\frac{\sin(\theta/2)\sin(\theta)}{|G(e^{i\theta},v)|}$$

$$\times\sin\left[\frac{\gamma}{2}(\Psi^{(e)}_{l00}+1)\right]\left[S_{1l}\cot\left(\frac{\pi}{2}\Psi^{(e)}_{l00}\right)+S_{2l}\csc\left(\frac{\pi}{2}\Psi^{(e)}_{l00}\right)\right]d\theta$$

$$+\sum_{m=-\infty}^{\infty}[S_{1l}+(-1)^mS_{2l}]\int_0^{\pi}\frac{\sin(\theta/2)\sin(\theta)}{|G(e^{i\theta},v)|}\cos\left[\left(m+\frac{1}{2}\right)\gamma\right]\delta(\Psi^{(e)}_{l00}-2m)\,d\theta\Big\}. \tag{50}$$

Terms occurring in these integrals are

$$(S_{kl})=\begin{pmatrix}-1 & 1 & -1 & 1 & 1 & -1 & 1 & -1\\ -1 & 1 & 1 & -1 & -1 & 1 & 1 & -1\end{pmatrix}, \tag{51}$$

$$\gamma(\theta,v)=2\tan^{-1}\left[\frac{[3-4v-\cos(\theta)]\sin(\theta)}{[1-2v-\cos(\theta)]^2}\right] \tag{52}$$

with $0 \le \gamma(\theta, v) \le \pi$ for $0 \le \theta \le \pi$,

$$\Phi_l(x_1,x_3,t,\chi)=\frac{x_1}{2H}\left[\left(\chi-\frac{a-1}{a+1}\right)\left(\frac{a+1}{a-1}-\chi\right)\right]^{\frac{1}{2}}-(-1)^l\frac{c_1t}{H(a^2-1)^{\frac{1}{2}}}\chi^{\frac{1}{2}}$$

$$+x_3(1-\chi)/2H\pm\tfrac{1}{2}(1+\chi), \tag{53}$$

$$\Psi_l(x_1,x_3,t,\chi)=\frac{c_1t}{H(a^2-1)^{\frac{1}{2}}}\chi^{\frac{1}{2}}-(-1)^l\frac{x_1}{2H}\left[\left(\chi-\frac{a-1}{a+1}\right)\left(\frac{a+1}{a-1}-\chi\right)\right]^{\frac{1}{2}}$$

$$\pm\tfrac{1}{2}(1-\chi)+x_3(1+\chi)/2H,$$

$$\Phi^{(e)}_{lpq}=2[\Phi_l-1-(1-\chi)p-2q]/(1+\chi),$$

$$\Psi^{(e)}_{lpq}=2[\Psi_l-1-(1-\chi)p-2q]/(1+\chi), \tag{54}$$

$$\Phi^{(d)}_{lpq}=2[\Phi_l+1+(1+\chi)p+2q]/(1-\chi),$$

$$\Psi^{(d)}_{lpq}=2[\Psi_l+1+(1+\chi)p+2q]/(1-\chi).$$

In (53) the upper sign applies for $l = 1$–4, the lower sign applies for $l = 5$–8 and x_3 is replaced with $-x_3$ for $l = 3, 4, 7, 8$. The coefficients $A_{pq}(\chi, \Phi)$ for $0 \leq p+q \leq 3$ are

$$
\begin{aligned}
A_{00} &= 1,\\
A_{10} &= i(\Phi-1+\chi)E^{(1)},\\
A_{01} &= -(1+\chi R^2)/(1+\chi),\\
A_{20} &= -\tfrac{1}{2}[\Phi^2-2\Phi(1-\chi)+1-3\chi+\chi^2](E^{(1)})^2+i(\Phi-1+\chi)E^{(2)},\\
A_{11} &= -i[\Phi(1+\chi R^2)/(1+\chi)-(3-2\chi)(1+\chi R^2)/(1+\chi)+\chi R^2]E^{(1)},\\
A_{02} &= (1+\chi R^2)^2/(1+\chi)^2,\\
A_{30} &= -\frac{i}{6}[\Phi^3-3\Phi^2(1-\chi)+3\Phi(1-3\chi+\chi^2)-(1-\chi)(1-6\chi+\chi^2)](E^{(1)})^3-[\Phi^2-2\Phi(1-\chi)\\
&\quad +1-3\chi+\chi^2]E^{(1)}E^{(2)}+i(\Phi-1+\chi)E^{(3)},\\
A_{21} &= \tfrac{1}{2}[\Phi^2(1+\chi R^2)/(1+\chi)-2\Phi(3-2\chi)(1+\chi R^2)/(1+\chi)+2\Phi\chi R^2\\
&\quad +(9-14\chi+4\chi^2)(1+\chi R^2)/(1+\chi)-5\chi(1-\chi)R^2](E^{(1)})^2\\
&\quad -i[\Phi(1+\chi R^2)/(1+\chi)-(3-2\chi)(1+\chi R^2)/(1+\chi)+\chi R^2]E^{(2)},\\
A_{12} &= i[\Phi(1+\chi R^2)^2/(1+\chi)^2+(3\chi-5)(1+\chi R^2)^2/(1+\chi)^2+2\chi R^2(1+\chi R^2)/(1+\chi)]E^{(1)},\\
A_{03} &= -(1+\chi R^2)^3/(1+\chi)^3.
\end{aligned}
\tag{55}
$$

The coefficients $A'_{pq}(\chi, \Phi)$ are obtained by replacing χ and Φ with $-\chi$ and $-\Phi$, respectively, and replacing $E^{(j)}$ with $-D^{(j)}$ while $R = R(\chi, \nu)$ remains unchanged in $A_{pq}(\chi, \Phi)$.

(*Received* 14 *July* 1970; *revised* 5 *October* 1970)

Абстракт—Определяется новая форма обыкновенного модального решения выражений высокой частоты для поведения бесконечной пластинкм под влиянием импульсивной линейной нагрузки. Используется изменение переменных для облегчения исследования ветвей уравнения частоты Рэлея-Ламба. Находятся точки ветвей, вокруг которых делаются аналитические продолжения, что приводит кновой форме модального решения и разделяет продольное и равнообъемное движение. Исследуются фронты особых волн, и определяются некоторые члены в остаточном решении, приближенные выражениями высокой частоты в рядах. Сравниваются эти результаты с известными решениями для полупространства. Метод можно применить к некоторым анизотропным материалам, но в данном случае, рассматривается однородная, изотропная пластинка.